CHEMISTRY
A EUROPEAN JOURNAL

FULL PAPER

DOI: 10.1002/chem.201203291

Organoruthenium Antagonists of Human A_3 Adenosine Receptors

Priyankar Paira,[a] Mun Juinn Chow,[b, c] Gopalakrishnan Venkatesan,[a] Vamsi Krishna Kosaraju,[b] Siew Lee Cheong,[a] Karl-Norbert Klotz,[d] Wee Han Ang,*[b] and Giorgia Pastorin*[a, c]

Abstract: Human A_3 adenosine receptor (hA_3AR) is a membrane-bound G protein-coupled receptor implicated in a number of severe pathological conditions, including cancer, in which it acts as a potential therapeutic target. To derive structure–activity relationships on pyrazolo–triazolo–pyrimidine (PTP)-based A_3AR antagonists, we developed a new class of organometallic inhibitors through replacement of the triazolo moiety with an organoruthenium fragment. The objective was to introduce by design structural diversity into the PTP scaffold in order to tune their binding efficacy toward the target receptor. These novel organoruthenium antagonists displayed good aquatic stability and moderate binding affinity toward the hA_3 receptor in the low micromolar range. The assembly of these complexes through a template-driven approach with selective ligand replacement at the metal center to control their steric and receptor-binding properties is discussed.

Keywords: adenosine · ligand design · nitrogen heterocycles · ruthenium · templated assembly

Introduction

Adenosine is an endogenous purine nucleoside that modulates a wide variety of physiological responses by interacting with specific adenosine receptors.[1] These receptors are widely distributed in mammalian tissues and have been classified into four different G-protein-coupled receptor subtypes, namely, A_1, A_{2A}, A_{2B}, and A_3 adenosine receptors.[2] There is growing evidence that suggests that the A_3 adenosine receptor (A_3AR) subtype is implicated in pathological conditions such as cardiac and cerebral ischemia, neurodegenerative diseases, and inflammatory pathologies, including rheumatoid arthritis and asthma.[3] Furthermore, A_3AR is overexpressed in some tumor cell lines, such as astrocytoma, B16-F10, A378 melanoma, and HL-60 leukemia,[4] as well as in solid tumors (e.g., a 2.3-fold increase in colon carcinomas), and this expression is correlated with disease progression.[5] Studies have established that this receptor could be a prospective therapeutic target in cancer therapy. Currently, the targeting of A_3AR in a clinical setting still presents a major challenge[6] because modulation of this receptor subtype may induce both pro- or antiapoptotic effects depending on the duration and the extent of activation/inactivation and the type of receptor binding.[1c]

The possible role of A_3AR modulation in the pathogenesis of such diseases has led to the advent of A_3AR antagonists as therapies for various pathophysiological conditions. In the past few years, there have been concerted efforts to develop different heterocyclic scaffolds as hA_3ARs antagonists. These scaffolds include pyridine and dihydropyridine analogues,[7] flavonoid,[8] isoquinoline,[9] triazoloquinazolines,[10] pyrazolo-[3,4-*c*] or -[4,3-*c*]quinolones,[11] and pyrazolo-[4,3-*e*]1,2,4-triazolo-[1,5-c]pyrimidines (**A**–**F**)[12] (Figure 1). Our group recently reported a new series of pyrazolo[4,3-*e*]-1,2,4-triazolo-[1,5-*c*]pyrimidines (PTP; Figure 2) centered on the replacement of the conventional furan ring at the C2 position with a 2-(*para*-substituted) phenyl ring and various substituents at the N5 and N8 positions. These new modifications enhanced the pharmacological profile of the antagonists significantly, with hA_3 affinity in the low nanomolar range and improved selectivity against the other adenosine receptor subtypes. It also provided a convenient replacement of the metabolically unstable furan ring.[13] Molecular modeling studies indicated stabilizing hydrogen-bonding interactions with the asparagine (Asn) 250

[a] Dr. P. Paira, G. Venkatesan, Dr. S.-L. Cheong, Assoc.Prof. G. Pastorin
Department of Pharmacy
National University of Singapore
3 Science Drive 2, Singapore 117543 (Singapore)
Fax: (+65) 6779 1554
E-mail: phapg@nus.edu.sg

[b] M. J. Chow, V. K. Kosaraju, Dr. W. H. Ang
Department of Chemistry
National University of Singapore
3 Science Drive 2, Singapore 117543 (Singapore)
Fax: (+65) 6779-1691
E-mail: chmawh@nus.edu.sg

[c] M. J. Chow, Assoc.Prof. G. Pastorin
NUS Graduate School for Integrative Sciences and Engineering
Center for Life Sciences (CeLS)
28 Medical Drive, 05-01, Singapore 117456 (Singapore)

[d] K.-N. Klotz
Institut für Pharmakologie und Toxikologie
Universität Würzburg, 97078 Würzburg (Germany)

Supporting information for this article is available on the WWW under http://dx.doi.org/10.1002/chem.201203291.

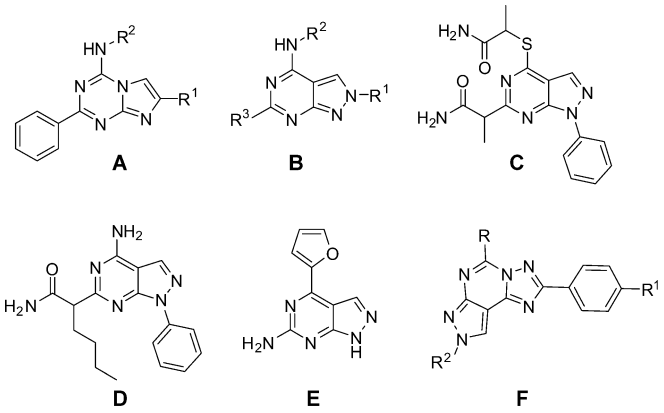

Figure 1. Examples of human A_3 adenosine receptor (hA_3AR) antagonists.

residue, π–π stacking interactions between the triazole ring and phenylalanine (Phe) 168 residue, and hydrophobic interactions with several other residues of the binding site.

A common feature in the vast majority of reported A_3AR antagonists is their flat multicyclic polyaromatic structure. While mapping the functional-group dependency on the PTP scaffold for studies on the structure–activity relationship, we observed that sterically encumbered planar aryl substituents at the C2 position improved antagonist binding (see Figure 2 for numbering order). We were therefore interested in exploring the effects of other substitutions, particularly hydrophobic nonplanar moieties that were structurally distinct from aryl rings, as a means of tuning antagonist–receptor interactions at the binding site. We sought to develop a facile method of introducing such structural elements into the PTP framework by using templated assembly of metal–ligand fragments (Figure 1).

The concept of applying organotransition-metal fragments as structural scaffolds for complex organic frameworks has been pursued for different purposes.[14] Meggers and co-workers demonstrated that highly potent active-site inhibitors of kinases can be developed by replacing the glycoside motif within staurosporine, a known kinase inhibitor, with different organoruthenium moieties.[15] In this manner, the ruthenium metal center played a structural role in the organization of the rigid metal–ligand framework.[16] Metzler-Nolte and co-workers investigated synthetic analogues of antibiotic platensimycin by substituting the complex tetracyclic cage component with isosteric organometallic fragments.[17] Dyson and co-workers developed a class of highly potent arene-functionalized metalloinhibitor of glutathione-*S*-transferase, which covalently binds at the enzyme dimer interface through their ruthenium (Ru^{II})–arene component.[18] We recently reported a class of selective organoruthenium inhibitor of protein tyrosine phosphatase 1B, designed to bind at the enzymatic active site while simultaneously interacting with the peripheral structural space.[19] The hexavalent Ru^{II} center enabled the rapid assembly of different ligand sets, thus giving rise to metalloinhibitors with differing structural characteristics and binding affinities. This increasingly prevalent use of ruthenium in the development of metallocomplexes capable of eliciting biological responses[20] is in part due to recent successes of ruthenium anticancer complexes in preclincal and clinical trials.[21] Notable examples include the antimetastatic NAMI-A and Ru^{II}–arene–PTA (RAPTA) series of complexes[22] and antitumoral KP1019 and {(η^6-arene)Ru^{II}} complexes with ethylenediammine ligands.[23] Ruthenium complexes are not known to cause systemic toxicities and are well tolerated in vivo,[24] which is in stark contrast to other heavy metals such as mercury, osmium, and cadmium.

Our strategy was to exploit organotransition-metal chemistry as a means of directly introducing unique structural elements into the PTP scaffold that are different from classical organic-based heterocycles. These structural elements would be organized around a [Ru]–PP scaffold (Figure 2)

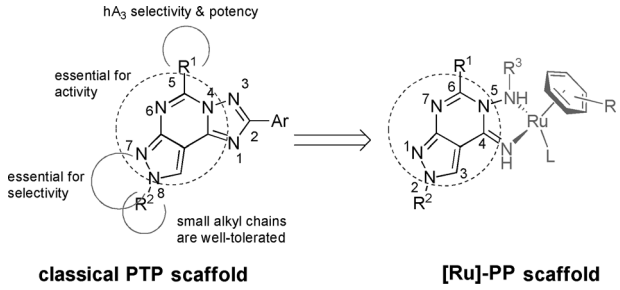

Figure 2. Design of A_3AR antagonists based on the PTP scaffold. PP = pyrazolo-[3,4-*d*]pyrimidine.

using chelating pyrazolo-[3,4-*d*]pyrimidine (PP) as a ligand. Therefore, ligands that are conformationally orthogonal to the [Ru]–PP metallacyle can be systematically introduced, thus allowing us to probe the receptor binding space within the immediate substrate-binding site. In this study, we developed this new class of organoruthenium hA_3AR antagonist and carried out docking and structure–activity relationship studies to ascertain the role of different structural elements in the binding mode at the hA_3 receptor subtype.

Results and Discussion

Design of organoruthenium PP scaffold: We adopted a template-driven approach to assemble the envisaged organoruthenium complexes as hA_3AR antagonists. Our key consideration was to design the PTP scaffold in a manner such that it would bind to organoruthenium precursors in good yield. The dimeric [{(η^6-arene)$RuCl_2$}$_2$] complex was utilized as the precursor because it is stable and easily prepared with a variety of different arene ligands. We retained the pyrazole ring on the PTP scaffold, which is responsible for the selective binding at the hA_3 receptor, but we retrosynthetically reduced the aryl–triazole ring into an α-hydrazine–imine bonding arrangement, so that it would readily chelate

the organoruthenium center. Reaction with [{(η^6-arene)-$RuCl_2$}$_2$] would result in cleavage of the dimer and displacement of a Cl ligand, thus inducing a positive charge at the metal center. This outcome would be accompanied by change in solvation properties, and we expected the final compound to precipitate readily from organic solvents upon formation. We also considered the fact that the arene ligand would be organized orthogonally from the remaining three coordination sites upon ligand binding and would provide the intended unique ligand disposition not easily achieved in a purely organic framework.

Synthesis and characterization: On the basis of these considerations, we designed a set of PTP mimetics as ligands, which would retain good interaction at the binding site of the receptor through the PP motif (as confirmed by the docking studies reported in the Supporting Information), while allowing facile coordination to the Ru^{II} through the α-hydrazine–imine chelate. Our strategy of preparing ligands **4a–f** is summarized in Scheme 1.

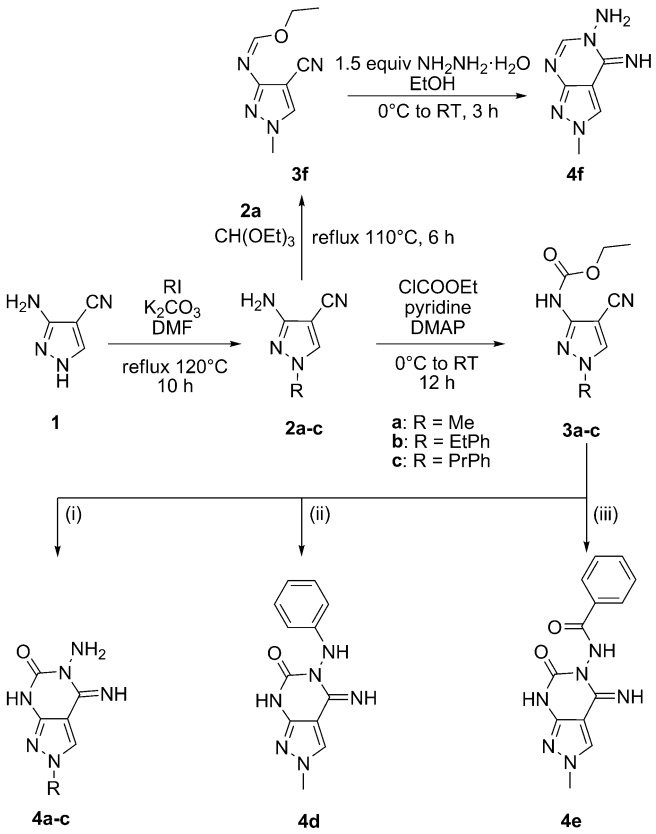

Scheme 1. Synthesis of 4-imino-(2-substituted)-2*H*-pyrazolo[3,4-*d*]-pyrimidine scaffolds (**4a–f**). DMAP = dimethylaminopyridine. i) 1.5 equiv $NH_2NH_2{\cdot}H_2O$, EtOH, reflux 80 °C, 6 h; ii) 1.5 equiv $PhCONHNH_2$, reflux 80 °C, 6 h; iii) 1.5 equiv $PhNHNH_2$, reflux 80 °C, 6 h.

Alkylation of 3-amino-4-pyrazolecarbonitrile **1** with alkyl or aryl iodide in dry DMF with dry potassium carbonate as a weak base led to N1-substituted regioisomer **2a–c** as a major product. 3-Amino-(N1-substituted)-4-pyrazolecarbonitriles **2a–c** were transformed into their corresponding carbamates (**3a–c**) through a reaction with ethyl chloroformate in pyridine at ambient temperature. A catalytic amount of DMAP was used as a cocatalyst to favor this acylation reaction. Carbamates **3** were subsequently treated with hydrazine hydrate in EtOH at 80 °C for 6 h to afford the 5-amino-4-imino-2-substituted-4,5-dihydro-2*H*-pyrazolo[3,4-*d*]pyrimidin-6(7*H*)-one (**4a–c**) in moderate yield. The structures of these compounds were readily confirmed by ^{1}H NMR and ESI-MS. A similar reaction protocol was adopted for the synthesis of substituted hydrazines. *N*-Carbamate **3a** was treated with phenylhydrazine and benzoic hydrazide in 2-methoxyethanol at 120 °C under reflux for 8 h to give 4-imino-2-methyl-5-(phenylamino)-4,5-dihydro-2*H*-pyrazolo-[3,4-*d*]pyrimidin-6(7*H*)-one (**4d**) and *N*-(4-imino-2-methyl-6-oxo-6,7-dihydro-2*H*-pyrazolo[3,4-*d*]pyrimidin-5(4*H*)-yl)-benzamide (**4e**) in good yields (Scheme 1). Ligands **4d** and **4e** were fully characterized by ^{1}H NMR and ESI-MS. Intermediate **2a** was also treated directly with triethyl orthoformate under reflux to give the imidate **3f**, which was further cyclized with hydrazine hydrate in EtOH at ambient temperature (Scheme 1).[25]

To study the Ru^{II}–ligand interaction and its binding affinities on human A_1, A_{2A}, and A_3 receptors, a new class of ruthenium complex [(η^6-arene)RuCl(κ^2-PP)]·Cl (**5–7**) was developed. The synthesis of the bis-amino complex containing a bidentate PP ligand [(η^6-cymene)RuCl(κ^2-**4a**)]·Cl (**5a**) was accomplished in one step starting from the Ru^{II} complex [{(η^6-cymene)$RuCl_2$}$_2$]. The precursor was treated with slight excess of ligand **4a** in MeOH at ambient temperature for 2 h to yield yellow microcrystalline **5a** in high yield (Scheme 2). The structure of this complex was fully characterized by ^{1}H NMR and ESI-MS. In general, the ^{1}H NMR resonances for the arene protons of the Ru^{II}–arene complexes were shifted downfield relative to the corresponding starting Ru^{II} dimers. There were also characteristic changes in the splitting pattern of the protons in the arene ligand. Upon ligand coordination, the C_{2v} symmetry of the complex was disrupted. In deuterated dimethyl sulfoxide (DMSO), **5a** exhibited four distinct doublets ($\delta = 5.45$–5.85 ppm) for cymene CH and two doublets ($\delta = 1.14$-1.23 ppm) for the isopropyl CH_3 group in the ^{1}H NMR spectra due to the formation of enantiomers. The ESI-MS spectrum of **5a** showed two significant peaks at *m*/*z* 451 and 415 for the $[M]^+$ and $[M-HCl]^+$ ions, respectively, as characterized by the unique Ru isotope pattern. After optimization of the reaction conditions for preparing **5a**, the scope of this chemical approach was expanded to include other arene fragments [{(η^6-benzene)$RuCl_2$}$_2$] and [{(η^6-triisopropylbenzene)$RuCl_2$}$_2$] and PP ligands **4a–f** to produce a series of Ru complexes **5–7** in high yields (Schemes 2 and 3). All the structures were characterized by their ^{1}H NMR and ESI-MS.

For the development of structurally different compounds, **5a** and **5f** were further treated with 1.1 equivalents of 1,3,5-triaza-7-phosphatricyclo[3.3.1.1]decane (PTA) in dry MeOH in an inert atmosphere for 2 h to afford the complexes [(η^6-

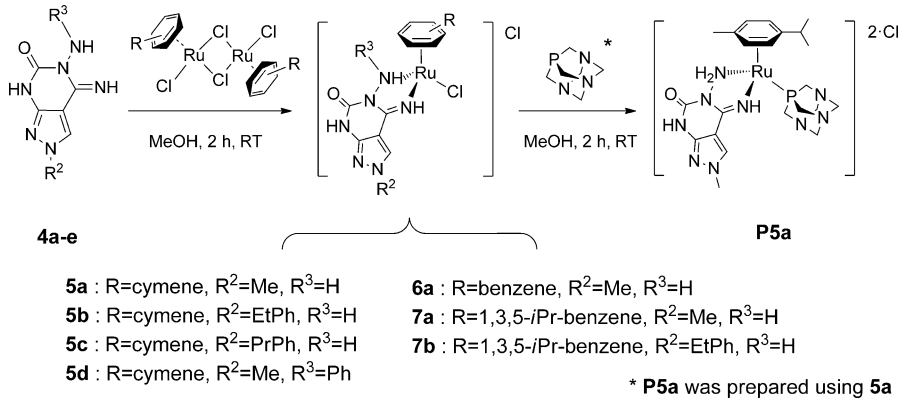

Scheme 2. Synthesis of [(η^6-arene)RuCl(κ^2-PP)]Cl (**5a–d**, **6a**, **7a**, and **7d**; PP = **4a–e**) and [(η^6-cymene)Ru(κ^2-**4a**)(PTA)]·2 Cl (**P5a**).

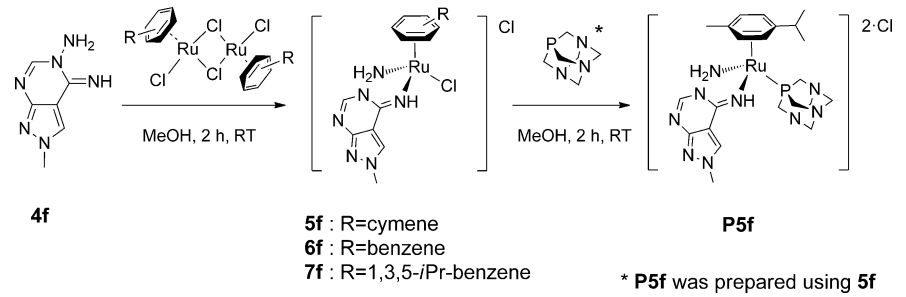

Scheme 3. Synthesis of [(η^6-arene)RuCl(κ^2-**4f**)]Cl (**5f**–**7f**) and [(η^6-cymene)Ru(κ^2-**4f**)(PTA)]·2 Cl (**P5f**).

cymene)Ru(PTA)(κ^2-**4a**)]·2 Cl (**P5a**) and [(η^6-cymene)Ru-(PTA)(κ^2-**4f**)]·2 Cl (**P5f**) in good yields (Schemes 2 and 3). The PTA ligand was introduced to increase the steric encumbrance at the organoruthenium component further. The structure of these complexes was determined by ^{1}H and ^{31}P{^{1}H} NMR and ESI-MS. The mass spectra of these compounds show a distinct peak at the $[M]^{2+}$ ion with the usual Ru isotope pattern. In the ^{31}P{^{1}H} NMR spectra, compounds **P5a** and **P5f** showed a singlet peak at $\delta = -34.5$ and -35.4 ppm, respectively, in comparison with RAPTA-C at $\delta = -36.2$ ppm.[26]

Structural determination of 5f and 7f: The structural determination of **5f** and **7f** in the solid state was carried out by using X-ray diffraction studies. Single crystals of **5f** and **7f** were grown by vapor diffusion of diethyl ether into a saturated solution of the compound in MeOH. Key crystallographic parameters were tabulated in Table 1. The Ru^{II} center assumed a piano-stool configuration supported by the facially bound arene ring, the bidentate PP moiety, and a Cl ligand (Figure 3). As far as we know, organoruthenium complexes containing such PTP scaffolds are unprecedented. The Ru–C and Ru–N bond lengths are of typical values and comparable with the known Ru^{II}–arene complexes containing diamino ligands (Table 2).[23c] The N1-Ru1-N2 bond angle of 76.89(16)° is significantly smaller than 90°, which indicated that the five-membered ring is strained. The Ru–ligand bond lengths in **7f** were also noticeably lengthened with respect to **5f**, presumably due to steric effects that arise from the bulky triisopropylbenzene arene ring. All in all, the structures vindicated our design approach to preposition the amido–hydrazide moiety for Ru^{II} chelation.

Aqueous stability: The aqueous stability of representative organoruthenium inhibitor **5a** was investigated by using UV/Vis spectroscopy to ensure that our organoruthenium antagonists would not spontaneously decompose or aquate upon dissolution in aqueous media, which would result in multiple species that could not be identified. Over a period of 24 h, the UV/Vis peak profile in water or 100 mM NaCl remained unchanged with the λ_{max} value, which remained constant, thus suggesting that the compound was stable (see Figure S1 in the Supporting Information). In the

Table 1. Selected X-ray crystallographic data for **5f** and **7f**.[a]

Complex	**5f**·2 CH_3OH	**7f**·H_2O
formula	$C_{18}H_{20}Cl_2N_6O_2Ru$	$C_{21}H_{32}Cl_2N_6ORu$
formula weight	534.45	556.50
T [K]	100(2)	223(2)
λ [Å]	0.71073	0.71073
crystal size [mm^3]	0.26×0.06×0.06	0.22×0.20×0.10
cystal system	monoclinic	monoclinic
space group	$C2/c$	$P2_1/n$
a [Å]	27.801(4)	13.4127(16)
b [Å]	9.2910(14)	14.2921(17)
c [Å]	17.537(3)	14.7053(18)
β [°]	94.383(3)	95.938(3)
V [Å^3]	4516.6(12)	2803.8(6)
Z	8	4
ρ_{calcd} [Mg m^{3-}]	1.572	1.318
μ [mm^{-1}]	0.957	0.771
Θ range [°]	2.31 to 27.50	1.96 to 25.00
data/restraints/parameters	5174/5/283	4929/15/301
max., min. transmission	0.9448 and 0.7889	0.9268 and 0.8486
final R indices	$R1 = 0.0623$	$R1 = 0.0760$
$[I>2\sigma(I)]$	$wR2 = 0.1146$	$wR2 = 0.1746$
R indices (all data)	$R1 = 0.0935$	$R1 = 0.1032$
	$wR2 = 0.1234$	$wR2 = 0.1878$
GOF on F^2	1.049	1.115
peak/hole [e Å^{-3}]	1.354 and −1.334	1.093 and −0.894

[a] $R = \Sigma||F_o|-|F_c||/\Sigma|F_o|$, $wR2 = \{\Sigma[w(F_o^2-F_c^2)^2]/\Sigma[w(F_o^2)^2]\}^{1/2}$. Goodness-of-fit (GOF) $= \{\Sigma[w(F_o^2-F_c^2)^2]/(n-p)\}^{1/2}$, where n is the number of data and p is the number of parameters refined.

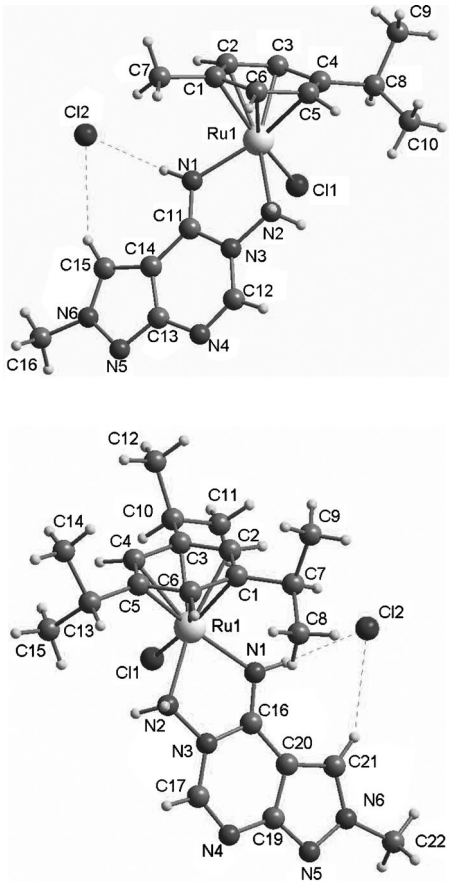

Figure 3. Molecular representations of **5f** (top) and **7f** (bottom). All the atoms are represented by spheres of arbitrary radii.

presence of 0.1 mM glutathione (GSH), to simulate an endogenous nucleophile, **5a** presented a shift in the λ_{max} value with an isosbestic point at $\lambda = 284$ nm. These observations suggested that although **5a** was stable under aqueous conditions, it could undergo ligand-exchange reactions with other nucleophiles. The reactivity of monocationic organoruthenium complexes were known to be mediated by the aquation.[27] Replacement of the chloride ligand by bulk water molecules yielded reactive Ru^{II}–aqua complexes that can undergo further ligand-substitution reactions particularly with the nucleophilic thiol-containing GSH. Indeed, the {(η^6-arene)Ru} moiety may modulate redox reactions of bound thiol groups, thus resulting in increased reactivity toward other nucleophiles.[28] It is, therefore, possible that such organoruthenium inhibitors can covalently bind to the target receptors to result in deactivation of the substrate binding site.

Studies on the structure–affinity relationship: The receptor-binding affinities of the synthesized ligands **4a–f** and Ru complexes **5–7** are summarized in Table 3. The affinity of the antagonists toward their receptors, expressed in CHO cells for human A_1, A_{2A}, and A_3 adenosine receptors and the corresponding adenylyl cyclase activity in CHO cells that expressed the A_{2B} receptors, was evaluated through measuring the displacement of selective radioligands, which were previously bound to the receptor expressed at the cell surface.[13]

Table 2. Comparison of bond lengths [Å] and angles [°] of **5f** and **7f**.

Complex	**5f**	**7f**
Ru1–N1	2.052(4)	2.065(6)
Ru1–N2	2.124(4)	2.129(6)
Ru1–Cl1	2.4051(13)	2.4142(19)
average Ru–C_{arene}	2.169–2.195	2.172–2.208
N2-Ru1-N1	76.89(16)	76.7(2)
N2-Ru1-Cl1	86.30(13)	84.01(18)
N1-Ru1-Cl1	82.01(12)	80.79(17)

The simple PP scaffold (e.g., **4f**) did not show any affinity toward any of the adenosine receptors. Moreover, no improvement was observed when a carbonyl group was introduced at the C6-position (e.g., **4a**; refer to Figure 2 for the numbering scheme of [Ru]-PP). This was also the case when groups bigger than a methyl group were introduced as N2 substituents, such as phenylethyl or phenylpropyl groups (i.e., **4b** and **4c**, respectively; Figure 2). This result indicated that, in contrast to the classical PTP scaffold (in which a clear inverse correlation existed between the molecular volume of the substituent at N8 and the affinity of the hA_3AR; Figure 2),[12] this position becomes less crucial. As soon as the free amino group in **4a** was substituted with a benzamide functionality, the affinity at both A_{2A} and A_3 adenosine receptors improved to within 14–20 μM ($K_i = >100$, 14.8, >100, and 19.8 μM for hA_1, hA_{2A}, hA_{2B}, and hA_3, respectively, for **4e**; Figure 2).

Table 3. Binding affinity of synthesized compounds at hA_1, hA_{2A}, and hA_3 adenosine receptors.[a]

	K_i [μM]			
	hA_1[b]	hA_{2A}[c]	hA_{2B}[d]	hA_3[e]
4a	>100	>100	>100	>100
4b	>100	>100	>100	>100
4c	>100	>100	>100	>100
4e	>100	14.8 (8.88–24.8)	>100	19.8 (15.3–25.6)
4f	>100	>100	>100	>100
5a	2.79 (1.94–4.01)	>100	>1	3.75 (2.32–6.06)
5b	18.1 (17.6–18.6)	51.2 (36.7–71.6)	>3	16.0 (11.5–22.3)
5c	5.00 (4.81–5.21)	10.1 (9.2–11.2)	>10	11.4 (7.17–18.2)
5d	>100	>100	>10	>100
5f	8.86 (7.45–10.5)	23.5 (16.5–33.6)	>10	17.9 (13.4–24.1)
6a	2.97 (1.84–4.8)	>100	>10	4.2 (3.04–5.82)
6f	>100	>100	>100	>100
7a	4.04 (2.33–7.01)	33.5 (20.9–53.6)	7.13 (5.04–10.1)	1.9 (1.12–3.23)
7f	5.01 (4.06–6.17)	13.8 (12.4–15.3)	>1	2.03 (1.1–3.72)
P5a	>30	>100	>10	20.1 (12.6–31.9)
P5f	>100	>100	>100	21.5 (15.7–29.4)

[a] Adenylyl cyclase activity of synthesized compounds at the $hA_{2B}AR$. [b] Displacement of specific [^{3}H]-CCPA binding at human A_1 receptors expressed in Chinese hamster ovary (CHO) cells ($n = 3$–6). [c] Displacement of specific [^{3}H]-5′-*N*-ethylcarboxamidoadenosine (NECA) binding at human A_{2A} receptors expressed in CHO cells ($n = 3$–6). [d] K_i values for inhibition of NECA-stimulated adenylyl cyclase activity in CHO cells ($n = 3$–6). [e] Displacement of specific [^{3}H]-2-(1-hexynyl)-*N*6-methyladenosine (HEMADO) binding at human A_3 receptors expressed in CHO cells ($n = 3$–6).

This phenomenon became even more evident when substitutions with Ru^{II}–arene moieties were introduced at the same position to give rise to Ru^{II} complexes [(η^6-arene)RuCl(κ^2-PP)]·Cl (**5**–**7**). Upon chelation, the Ru center formed a five-membered metallacycle with the PP ligand, which spatially mimicked the triazole unit in the PTP scaffold (also confirmed by the docking studies reported in the Supporting Information). Among the Ru derivatives, those bearing a carbonyl group to correspond to the C6-position and a methyl group at the N2-position of the PP ligand showed the best hA_3 affinity values, which were all in the low micromolar range (e.g., for hA_3, K_i = 3.75, 4.2, and 1.9 μM for **5a**, **6a**, and **7a**, respectively; Figure 2). The only exception to this observation was represented by the concurrent substitution at the N5-position with an additional aromatic ring (for hA_3, K_i > 100 μM for **5d**; Figure 2), which presumably was responsible for excessive steric hindrance at the binding site.

The introduction of Ru^{II}–arene moieties onto the original PP scaffold was associated with a more influential role of the concurrent substituent at the N2-position. Indeed, a similar trend for the PTP moiety was observed, because less sterically encumbered groups (e.g., the methyl group as in **5a**, **7a**, and **7f**; Figure 2) were more favorable than bulkier groups (e.g., phenylethyl and phenylpropyl; **5b** and **5c**, respectively; Figure 2). This suggested that the spatial encumbrance of the Ru moiety provided a more favorable interaction at the hA_3AR relative to the uncoordinated PP ligand.

The substituents on the arene ligand were varied to examine their influence on the binding affinity at the hA_3AR relative to their parent complexes. Unsubstituted η^6-benzene did not influence the pharmacological profile of the complexes because **6f** remained inactive and **6a**, containing a C6-carbonyl group (Figure 2), showed a moderate affinity. However, the replacement of the benzene ring with a η^6-cymene or η^6-triisopropylbenzene functionality enhanced the affinity and, in a few cases, also the selectivity toward hA_3AR. For example, Ru^{II} complexes containing η^6-cymene exhibited a remarkable increase in the affinity profile, even in the absence of the C6-carbonyl group (e.g., for **5f** K_i = 8.86, 23.5, and 17.9 μM for hA_1, hA_{2A}, and hA_3, respectively, versus **6f** with K_i = >100, >100, >100, and >100 μM for hA_1, hA_{2A}, hA_{2B}, and hA_3, respectively; Figure 2). In particular, the introduction of η^6-triisopropylbenzene, provided that a C6-carbonyl group and a methyl group at N2 were concurrently present, was responsible for the best affinity at the hA_3AR and a slight increase in selectivity over the other adenosine receptors (e.g., K_i = 1.9, 2.13, 17.6, and 3.8 μM for hA_3, hA_1/hA_3, hA_{2A}/hA_3, and hA_{2B}/hA_3, respectively, for **7a**; Figure 2).

Lastly, the chloride ligand was replaced with the strong σ-donor PTA species to tune the steric bulk around the Ru^{II} center. Upon substitution, a 1.2–5.6-fold decrease in the binding affinities were observed. The fact that there was only a slight decrease (1.2–5.6-fold) in the affinity profile suggests that the sterically encumbered PTA species would be accommodated (as observed in the docking studies and reported in Figure S25 of the Supporting Information) into the receptor binding pocket. Curiously, **P5a** and **P5f** displayed a significant increase in selectivity toward hA_3AR (e.g. **P5a** with K_i = >30, >100, >100, and 20.1 μM for hA_1, hA_{2A}, hA_{2B}, and hA_3, respectively, versus **5a** with K_i = 2.79, >100, >1.0, and 3.75 μM for hA_1, hA_{2A}, hA_{2B}, and hA_3, respectively; Figure 2). This suggested that substitutions at the chloride position could be further explored to increase the selectivity at the receptor of interest.

Overall, this structure–activity relationship study confirmed that the Ru^{II}–arene moieties increased affinity at hA_3AR relative to the uncoordinated PP ligand. When optimal substituents were introduced into the Ru^{II}–arene complexes (see Figure 2; namely 1) a 6-carbonyl unit, 2) a small alkyl group at N2, and 3) a η^6-triisopropylbenzene ligand), new antagonists with low micromolar affinity at the human A_3 adenosine receptor and a discrete selectivity over the other adenosine-receptor subtypes would be derived.

Conclusion

We investigated a series of Ru^{II}–arene complexes that contain PP chelating ligands to explore the effect of altering the nature of the bulky groups at the 2-aryltriazole position on PTP. The binding affinity profiles indicated that sterically hindered Ru^{II}–arene complexes were well-tolerated at the binding site and exhibited moderate affinity toward the hA_3AR. In particular, [(η^6-triisopropylbenzene)Ru^{II}] complexes **7a** and **7f** exhibited the best profile in terms of both affinity and selectivity at hA_3AR and good aqueous solubility, overcoming a limitation in the classical tricyclic-PTP scaffold. Our study paves the way for Ru^{II}–arene complexes as promising hA_3AR antagonists.

Experimental Section

Materials and methods: Reactions were monitored by TLC analysis on silica gel (precoated 60 F254 Merck plate). All the organometallic reactions were carried out in a nitrogen atmosphere. Complexes [{(η^6-cymene)$RuCl_2$}$_2$], [{(η^6-benzene)$RuCl_2$}$_2$], and [{(η^6-triisopropylbenzene)$RuCl_2$}$_2$] were prepared as described elsewhere.[29] All the other chemicals were commercial products and were purchased from Sigma-Aldrich. Column chromatography was performed on silica gel 60 (Merck, 70–230 mesh). IR spectra of the compounds (2 mg, KBr tablets) were recorded on a Spectrum100 FTIR machine (PerkinElmer). The compounds were dissolved in HPLC-grade MeOH for the determination of a mass-to-charge ratio m/z on a LCQ Finnigan MAT electrospray mass spectrometer. ^1H, $^{13}C\{^1H\}$, and $^{31}P\{^1H\}$ NMR spectra were determined in deuterated MeOH (CD_3OD) or deuterated dimethyl sulfoxide ([D_6]DMSO) on Bruker DPX Ultrashield NMR (300 or 400 MHz) spectrometers. Chemical shifts were given in parts per million δ downfield relative to the central peak of the solvents, and J values (coupling constants) were given in Hz. The following abbreviations were used: s = singlet, d = doublet, dd = double doublet, t = triplet, sep = septet, m = multiplet, br = broad.

General procedure for the preparation of *N*-alkylpyrazoles 2: Alkyl iodide (1.2 mmol) was added dropwise to a suspension of 3-amino-4-pyrazolecarbonitriles **1** (100 mg, 0.93 mmol) and anhydrous potassium carbonate (1.5 mmol, 191.8 mg) in DMF (5 mL). The reaction mixture was

heated to reflux at 100 °C for 12 h. After the complete conversion of the starting material by monitoring with TLC analysis, the reaction mixture was poured into ice cold water and extracted with ethyl acetate (5× 25 mL). The organic layers were recombined, dried over Na_2SO_4, filtered, and concentrated at reduced pressure to afford the alkylated pyrazoles **2a–c** as an inseparable mixture of N1 and N2 isomers. The pure N1 isomer was further purified by fractional crystallization from ethyl acetate/hexane.

3-Amino-1-methyl-1*H*-pyrazole-4-carbonitrile (2a): Product was obtained as a pale yellow solid (67.3%, 76 mg). ^{1}H NMR (300 MHz, [D$_6$]DMSO): δ=3.51 (s, 3H; Me), 6.52 (s, 2H; NH$_2$), 7.49 ppm (s, 1H; pyrazolo-*H*); ^{13}C{^{1}H} NMR (300 MHz, [D$_6$]DMSO): δ=35.6 (Me), 73.1 (C), 116.3 (C), 140.9 (CH), 152.5 ppm (C); ESI-MS (MeOH): *m*/*z*: 123.0 [*M*+H]$^+$.

3-Amino-1-phenethyl-1*H*-pyrazole-4-carbonitrile (2b): Product was obtained as a yellow solid (76.2%, 149 mg). ^{1}H NMR (300 MHz, CD$_3$OD): δ=3.08 (t, *J*=7.2 Hz, 2H; CH$_2$), 4.15 (t, *J*=6.9 Hz, 2H; CH$_2$), 7.09–7.29 (m, 5H; Ph), 7.56 ppm (s, 1H; CH); ESI-MS (MeOH): *m*/*z*: 213.0 [*M*+H]$^+$.

3-Amino-1-(3-phenylpropyl)-1*H*-pyrazole-4-carbonitrile (2c): Product was obtained as a brown solid (82.2%, 172 mg). ^{1}H NMR (300 MHz, CD$_3$OD): δ=2.03–2.14 (m, 2H; CH$_2$), 2.56–2.65 (m, 2H; CH$_2$), 3.92–3.97 (m, 2H; CH$_2$), 7.18 (d, *J*=5.7 Hz, 2H; Ph), 7.28 (t, *J*=7.2 Hz, 3H; Ph), 7.51 (s, 2H; NH$_2$), 7.84 ppm (s, 1H; CH); ESI-MS (MeOH): *m*/*z*: 227.0 [*M*+H]$^+$.

General procedure for the synthesis of pyrazole-3-yl-carbamate 3: Pyridine (1 mL) was added to 3-amino-(N1-substituted)-4-pyrazolecarbonitriles **2** (0.491 mmol) and a catalytic amount of DMAP in a two-necked round-bottom flask at 0 °C. The solution was stirred in an inert atmosphere. Ethyl chloroformate (1.3 equiv) was added dropwise to the reaction mixture, which was further stirred for 10 h. After the complete consumption of the starting material, as monitored by TLC analysis, the reaction mixture was poured into ice-cold water and extracted with ethyl acetate (5×25 mL). The organic layers were recombined, dried over Na_2SO_4, filtered, and concentrated at reduced pressure. The residue was crystallized from ethyl acetate/hexane mixture.

Ethyl 4-cyano-1-methyl-1*H*-pyrazol-3-ylcarbamate (3a): Product was obtained as a yellow solid (87.2%, 83.2 mg). ^{1}H NMR (300 MHz, [D$_6$]DMSO): δ=1.25 (t, *J*=7.2 Hz, 3H; Me), 3.67 (s, 3H; NMe), 4.18 (q, *J*=6.9 Hz, 2H; O–CH$_2$), 7.95 (s, 1H; pyrazolo-*H*), 10.09 ppm (s, 1H; CONH); ^{13}C{^{1}H} NMR (300 MHz, [D$_6$]DMSO): δ=15.3 (Me), 37.2 (N–Me), 62.8 (OCH$_2$), 87.4 (C–CN), 114.2 (CN), 142.0 (C), 142.1 (CH), 154.0 ppm (CONH); ESI-MS (MeOH): *m*/*z*: 195.0 [*M*+H]$^+$.

Ethyl 4-cyano-1-phenethyl-1*H*-pyrazol-3-ylcarbamate (3b): Product was obtained as an orange solid (71.8%, 102 mg). ^{1}H NMR (300 MHz, CD$_3$OD): δ=1.23–1.30 (m, 3H; Me), 3.14 (t, *J*=7.2 Hz, 2H; CH$_2$), 4.12 (q, *J*=7.2 Hz, 2H; O–CH$_2$), 4.28–4.32 (m, 2H; CH$_2$), 7.18–7.22 (m, 5H; Ph), 7.87 (s, 1H; pyrazolo-*H*), 8.55 ppm (s, 1H; CONH); ESI-MS (MeOH): *m*/*z*: 285.0 [*M*+H]$^+$.

Ethyl 4-cyano-1-(3-phenylpropyl)-1*H*-pyrazol-3-ylcarbamate (3c): Product was obtained as a yellow solid (74.2%, 111 mg). ^{1}H NMR (300 MHz, CD$_3$OD): δ=1.23–1.30 (m, 3H; Me), 2.16 (m, 2H; CH$_2$), 2.56–2.66 (m, 2H; CH$_2$), 4.01–4.03 (t, *J*=7.5 Hz, 2H; CH$_2$), 4.10–4.29 (m, 2H; OCH$_2$), 7.18–7.28 (m, 5H; Ph), 8.14 (s, 1H; pyrazolo-*H*), 8.55 ppm (s, 1H; CONH); ESI-MS (MeOH): *m*/*z*: 299.0 [*M*+H]$^+$.

General procedure for the preparation of pyrazolopyrimidine-6-ones 4a–c: *N*-Carbamates **3** (0.5 mmol) was dissolved in dry EtOH (2 mL) and the solution was poured in a two-necked round-bottom flask in a nitrogen atmosphere. Hydrazine hydrate (1.5 equiv) was added to the reaction mixture dropwise, which was heated to reflux at 80 °C for 6 h. A white precipitate was formed from the reaction mixture and filtered. The crude solid was washed with acetone and recrystallized from MeOH/hexane.

5-Amino-4-imino-2-methyl-4,5-dihydro-2*H*-pyrazolo[3,4-*d*]pyrimidin-6-(7*H*)-one (4a): Product was obtained as a white solid (57.8%, 52 mg). ^{1}H NMR (300 MHz, [D$_6$]DMSO): δ=3.59 (s, 3H; NMe), 5.31 (s, 2H; NH$_2$), 7.85 (s, 1H; pyrazolo-*H*), 8.03 (s, 1H; CONH), 8.82 ppm (s, 1H; C=NH), ^{13}C{^{1}H} NMR (300 MHz, [D$_6$]DMSO): δ=33.7 (N–Me), 91.9 (C–CN), 134.2 (CH), 153.0 (C), 154.5 (C=NH), 155.1 ppm (CONH); IR (KBr): $\tilde{\nu}$=3699, 3286, 2180, 1692, 1627, 1570, 760 cm^{-1}; ESI-MS (MeOH): *m*/*z*: 181.0 [*M*+H]$^+$; HRMS (ESI): *m*/*z* calcd for $C_6H_8N_6O$+Na$^+$: 203.0657 [*M*+Na$^+$]; found: 203.0650.

5-Amino-4-imino-2-phenethyl-4,5-dihydro-2*H*-pyrazolo[3,4-*d*]pyrimidin-6(7*H*)-one (4b): Product was obtained as a white solid (58.6%, 87.5 mg). ^{1}H NMR (400 MHz, [D$_6$]DMSO): δ=3.05 (t, *J*=7.2 Hz, 2H; CH$_2$), 4.24 (t, *J*=7.2 Hz, 2H; CH$_2$), 5.33 (br, 2H; NH$_2$), 7.17–7.28 (m, 5H; Ph), 7.93 (s, 1H; pyrazolo-*H*), 8.25 (s, 1H; CONH), 9.08 ppm (s, 1H; C=NH); IR (KBr): $\tilde{\nu}$=3600, 3350, 2342, 1644, 1620, 1539, 820 cm^{-1}; ESI-MS (MeOH): *m*/*z*: 271 [*M*+H]$^+$; HRMS (ESI): *m*/*z* calcd for $C_{13}H_{14}N_6O$+H$^+$: 271.1307 [*M*+H$^+$]; found: 271.1302.

5-Amino-4-imino-2-(3-phenylpropyl)-4,5-dihydro-2*H*-pyrazolo[3,4-*d*]pyrimidin-6(7*H*)-one (4c): Product was obtained as a white solid (52.6%, 74.6 mg). ^{1}H NMR (400 MHz, [D$_6$]DMSO): δ=2.00 (p, *J*=7.2 Hz, 2H; CH$_2$), 2.55 (t, *J*=7.2 Hz, 2H; CH$_2$), 4.02 (t, *J*=7.2 Hz, 2H; CH$_2$), 5.29 (s, 2H; NH$_2$), 7.16–7.30 (m, 5H; Ph), 7.90 (s, 1H; pyrazolo-*H*), 8.02 (s, 1H; CONH), 8.82 ppm (s, 1H; C=NH); IR (KBr): $\tilde{\nu}$=3625, 3327, 3249, 2647, 1667, 1630, 1515, 1142, 782 cm^{-1}; ESI-MS (MeOH): *m*/*z*: 285 [*M*+H]$^+$; HRMS (ESI): *m*/*z* calcd for $C_{14}H_{16}N_6O$+H$^+$: 285.1464 [*M*+H$^+$]; found: 285.1461.

4-Imino-2-methyl-5-(phenylamino)-4,5-dihydro-2*H*-pyrazolo-[3,4-*d*]pyrimidin-6(7*H*)-one (4d): Phenylhydrazine (0.05 mL, 1.5 equiv) was added dropwise to ligand **3a** (0.25 mmol, 48.5 mg) in dry 2-methoxyethanol (2 mL) in a two-necked round bottom flask under nitrogen. The reaction mixture was heated to reflux at 120 °C for 8 h. A white solid precipitated and was filtered. The crude product was washed with acetone and recrystallized from MeOH/hexane as a white solid (52.6%, 33.7 mg). ^{1}H NMR (400 MHz, [D$_6$]DMSO): δ=3.61 (s, 3H; N–Me), 6.63 (d, *J*=7.6 Hz, 2H; CH), 6.85 (t, *J*=7.2 Hz, 1H; CH), 7.19 (t, *J*=7.2 Hz, 2H; CH), 7.94 (s, 1H; pyrazole-*H*), 8.42 (s, 1H; NH), 8.63 (s, 1H; NHCO), 9.05 ppm (s, 1H; C=NH); IR (KBr): $\tilde{\nu}$=3511, 3427, 3246, 2984, 1670, 1631, 1602, 1515, 1495, 766 cm^{-1}; ESI-MS (MeOH): *m*/*z*: 257.0 [*M*+H]$^+$; HRMS (ESI): *m*/*z* calcd for $C_{12}H_{12}N_6O$+H$^+$: 257.1151 [*M*+H$^+$]; found: 257.1153.

***N*-(4-Imino-2-methyl-6-oxo-6,7-dihydro-2*H*-pyrazolo[3,4-*d*]-pyrimidin-5(4*H*)-yl)benzamide (4e)**: Ligand **3a** (0.21 mmol, 40 mg) was dissolved in 2-methoxyethanol (2 mL) and the solution was taken in a two-necked round bottom flask under nitrogen atmosphere. Benzhydrazide (32 mg, 1.5 equiv) was added to the reaction mixture, which was heated to reflux at 120 °C for 8 h. A white solid precipitated and was filtered. The crude product was washed with acetone and recrystallized from MeOH/hexane as a white solid (56.2%, 32.9 mg). ^{1}H NMR (300 MHz, [D$_6$]DMSO): δ= 3.62 (s, 3H; Me), 7.48–7.88 (m, 5H; CH), 7.92 (s, 1H; CH), 8.02 (s, 1H; NHCO), 8.04 (s, 1H; NHCO), 8.47 ppm (s, 1H; NH); IR (KBr): $\tilde{\nu}$= 3627, 3426, 3257, 1739, 1670, 1629, 1542, 788 cm^{-1}; ESI-MS (MeOH): *m*/*z*: 285 [*M*+H]$^+$; HRMS (ESI): *m*/*z* calcd for $C_{13}H_{12}N_6O_2$+H$^+$: 285.1100 [*M*+H$^+$]; found: 285.1082.

4-Imino-2-methyl-2*H*-pyrazolo[3,4-*d*]pyrimidin-5(4*H*)-amine (4f): Hydrazine hydrate (0.25 mL, 0.5 mmol) was added to a cold (0–5 °C) solution of intermediate **3f** in EtOH (10 mL). The mixture was stirred at room temperature for 5 h in an inert atmosphere. The resulting precipitate was filtered and washed with EtOH to provide **4f** as a white solid (82.5%, 76 mg). ^{1}H NMR (300 MHz, [D$_6$]DMSO): δ=3.80 (s, 3H; NMe), 5.54 (s, 2H; NH$_2$), 7.65 (s, 1H; C=NH), 7.98 (s, 1H; pyrazole-*H*), 8.04 (s, 1H; CH=N); ^{13}C NMR (300 MHz, [D$_6$]DMSO): δ=34.7 (N–Me), 104.9 (*C*-C=NH), 134.7 (CH-pyrazole), 148.6 (C), 151.4 (CH), 152.6 ppm (C=NH); IR (KBr): $\tilde{\nu}$=3457, 3286, 2938, 2140, 1662, 1609, 1551, 1229, 1157, 855, 767 cm^{-1}; ESI-MS (MeOH): *m*/*z*: 165.0 [*M*+H]$^+$; HRMS (ESI): *m*/*z* calcd for $C_6H_8N_6$+H$^+$: 165.0889 [*M*+H$^+$]; found: 165.0877.

General procedure for the preparation of ruthenium(II)/pyrazolo–pyrimidine complexes 5a–d, 5f, 6a, 6f, 7a, 7b, and 7f: All the compounds are synthesized by using a similar procedure. Typically, ligand **4a–d** or **4f** (2.1 equiv) was dissolved in dry MeOH (4 mL) and added to [{(η^6-cymene)RuCl$_2$}$_2$] in dry MeOH (3 mL). The solution immediately changed from red to brown/violet and was stirred at room temperature for 2 h. After complete conversion of the reagents, monitored by using TLC analysis, the product was precipitated with excess of diethyl ether. The crude

product was further washed with diethyl ether followed by acetone to yield the final product as a yellow–orange powder.

[(η^6-cymene)RuCl(κ^2-4a)]·Cl (5a): [{(η^6-cymene)$RuCl_2$}$_2$] (10 mg, 16 μmol) and **4a** (2.1 equiv, 34 μmol, 6.1 mg) were used. The solution turned from red to yellow–brown after stirring for 2 h. The product was obtained as a pale-yellow solid (88.5%, 14.0 mg) with HPLC purity (96.4%, eluent: 80% ACN/H_2O, R_t = 1.74 min). ^{1}H NMR (400 MHz, [D_6]DMSO): δ = 1.14(d, J=7.2 Hz, 3H; Me_2CH), 1.23 (d, J = 6.8 Hz, 3H; Me_2CH), 2.15 (s, 3H; Me), 2.84 (sep, J = 6.8 Hz, 1H; CH), 3.75 (s, 3H; NMe), 5.45 (d, J = 6.0 Hz, 1H; CH-cymene), 5.67 (br, 2H; CH-cymene), 5.85 (d, J = 6.0 Hz, 1H; CH-cymene), 7.80 (d, J = 9.6 Hz, 1H; NH), 8.07 (s, 1H; CH), 9.79 (d, J = 10.4 Hz, 1H; NH), 10.08 (s, 1H; NHCO), 12.77 ppm (br, 1H; NH); IR (KBr): $\tilde{\nu}$ = 3733, 3647, 3029, 1732, 1667, 1614, 1355, 1221, 1177, 821 cm^{-1}; ESI-MS (MeOH): m/z: 451.0 $[M]^+$, 415 $[M-HCl]^+$; HRMS (ESI): m/z calcd for $[C_{16}H_{22}N_6ORuCl-HCl]^+$: 415.0820 $[M-HCl]^+$; found: 415.0779.

[(η^6-cymene)RuCl(κ^2-4b)]·Cl (5b): [{(η^6-cymene)$RuCl_2$}$_2$] (10 mg, 16 μmol) and **4b** (2.1 equiv, 34 μmol, 9.2 mg) were used. The solution turned from red to yellow–brown after stirring for 2 h. The product was obtained as a brown solid (82.4%, 15.5 mg) with HPLC purity (99.8%, eluent: 80% ACN/H_2O, R_t: 2.04 min). ^{1}H NMR (400 MHz, [D_6]DMSO): δ = 1.12 (d, J = 6.8 Hz, 3H; Me_2CH), 1.21 (d, J = 6.8 Hz, 3H; Me_2CH), 2.12 (s, 3H; Me), 2.80 (sep, J = 6.8 Hz, 1H; CH), 3.00 (t, J = 7.2 Hz, 2H; CH_2), 4.14 (t, J = 8.0 Hz, 2H; CH_2), 5.35 (d, J = 5.6 Hz, 1H; CH-cymene), 5.60 (br, 1H; CH-cymene), 5.79 (d, J = 6.0 Hz, 1H; CH-cymene), 5.83 (d, J = 5.2 Hz, 1H; CH-cymene), 7.17–7.25 (m, 5H; Ph), 7.27 (2 brs, 2H; NH), 7.79 (s, 1H; CH), 8.55 (s, 1H; NHCO), 9.51 ppm (d, J = 10.2 Hz, 1H; NH); IR (KBr): $\tilde{\nu}$ = 3640, 3349, 3058, 2930, 1726, 1664, 1442, 1213, 1127, 1052, 781 cm^{-1}; ESI-MS (MeOH): m/z: 540.9 $[M]^+$, 504.8 $[M-HCl]^+$; HRMS (ESI): m/z calcd for $[C_{23}H_{28}N_6ORuCl-HCl]^+$: 505.1289 $[M-HCl]^+$; found: 505.1289.

[(η^6-cymene)RuCl(κ^2-4c)]·Cl (5c): [{(η^6-cymene)$RuCl_2$}$_2$] (10 mg, 16 μmol) and **4c** (2.1 equiv, 34 μmol, 9.7 mg) were used. The solution turned from red to yellow–brown after stirring for 2 h. The product was obtained as a brown solid (92.2%, 17.7 mg) with HPLC purity (99.8%, eluent: 80% ACN/H_2O, R_t: 2.17 min). ^{1}H NMR (300 MHz, [D_6]DMSO): δ = 1.14 (d, J = 6.9 Hz, 3H; Me_2CH), 1.22 (d, J = 6.3 Hz, 3H; Me_2CH), 2.03 (m, 2H; CH_2), 2.15 (s, 3H; Me), 2.58 (m, 2H; CH_2), 2.83 (m, 1H; CH), 4.14 (m, 2H; CH_2), 5.45 (d, J = 5.4 Hz, 1H; CH-cymene), 5.67 (s, 2H; CH-cymene), 5.86 (d, J = 5.7 Hz, 1H; CH-cymene), 7.15–7.25 (m, 5H; Ph), 7.79 (d, J = 8.7 Hz, 1H; NH), 8.10 (s, 1H; CH), 9.80 (d, J = 9.0 Hz, 1H; NH), 10.12 (s, 1H; NHCO), 12.72 ppm (s, 1H; NH); IR (KBr): $\tilde{\nu}$ = 3612, 3340, 3042, 2720, 1712, 1624, 1229, 1156, 792 cm^{-1}; ESI-MS (MeOH): m/z: 554.8 $[M]^+$, 518.8 $[M-HCl]^+$; HRMS (ESI): m/z calcd for $[C_{24}H_{30}N_6ORuCl-HCl]^+$: 519.1446 $[M-HCl]^+$; found: 519.1449.

[(η^6-cymene)RuCl(κ^2-4d)]·Cl (5d): Complex [{(η^6-cymene)$RuCl_2$}$_2$] (10 mg, 16 μmol) and **4d** (2.1 equiv, 34 μmol, 8.7 mg) were used. The solution turned from red to deep violet after stirring for 2 h. The product was obtained as a black solid (87.4%, 16.0 mg) with HPLC purity (98.5%, eluent: 80% ACN/H_2O, R_t: 2.23 min). ^{1}H NMR (300 MHz, CD_3OD): δ = 1.23 (d, J = 7.2 Hz, 3H; Me_2CH), 1.30 (br, 3H; Me_2CH), 2.23 (s, 3H; Me), 2.46–2.51 (m, 1H; CH), 4.03 (s, 3H; NMe), 6.01 (d, J = 5.7 Hz, 1H; CH-cymene), 6.16 (d, J = 6.0 Hz, 1H; CH-cymene), 6.23 (d, J = 5.7 Hz, 1H; CH-cymene), 6.61 (d, J = 6.3 Hz, 1H; CH-cymene), 7.09 (s, 1H; CH), 7.77–7.81 (m, 2H; CH), 7.89–7.92 (m, 1H; CH), 8.21 (d, J = 6.6 Hz, 2H; CH), 8.35 ppm (s, 1H; NHCO); IR (KBr): $\tilde{\nu}$ = 3631, 3427, 3022, 2942, 1653, 1597, 1446, 1034, 878, 758 cm^{-1}; ESI-MS (MeOH): m/z: 527.4 $[M]^+$, 491.4 $[M-HCl]^+$; HRMS (ESI): m/z calcd for $[C_{22}H_{26}N_6ORuCl-HCl]^+$: 491.1133 $[M-HCl]^+$; found: 491.1154.

[(η^6-cymene)RuCl(κ^2-4f)]·Cl (5f): Complex [{(η^6-cymene)$RuCl_2$}$_2$] (10 mg, 16 μmol) and **4f** (2.1 equiv, 34 μmol, 5.6 mg) were used. The solution turned from red to yellowish orange after stirring for 2 h. The product was obtained as a deep-yellow solid (86.2%, 13.4 mg) with HPLC purity (99.8%, eluent: 80% ACN/H_2O, R_t: 1.99 min). ^{1}H NMR (400 MHz, [D_6]DMSO): δ = 1.16 (d, J = 6.8 Hz, 3H; Me_2CH), 1.23 (d, J = 6.8 Hz, 3H; Me_2CH), 2.18 (s, 3H; Me), 2.88 (sep, J = 6.8 Hz, 1H; CH), 4.04 (s, 3H; NMe), 5.49 (d, J = 5.6 Hz, 1H; CH-cymene), 5.72 (d, J = 6.0 Hz, 1H; CH-cymene), 5.79 (d, J = 6.0 Hz, 1H; CH-cymene), 5.96 (d, J = 6.0 Hz, 1H; CH-cymene), 7.97 (s, 1H; CH), 8.55 (s, 1H; CH), 8.72 (d, J = 8.0 Hz, 1H; NH), 10.05 (s, 1H; NH), 11.12 ppm (d, J = 8.0 Hz, 1H; NH); IR (KBr): $\tilde{\nu}$ = 3465, 3249, 3118, 2966, 1662, 1608, 1542, 1425, 1230, 1174, 821 cm^{-1}; ESI-MS (MeOH): m/z: 435.0 $[M]^+$, 399.0 $[M-HCl]^+$; HRMS (ESI): m/z calcd for $[C_{16}H_{22}N_6RuCl-HCl]^+$: 399.0871 $[M-HCl]^+$; found: 399.0870; single crystals suitable for X-ray diffraction studies were obtained by vapor diffusion of diethyl ether into a saturated solution of the compound in MeOH.

[(η^6-benzene)RuCl(κ^2-4a)]·Cl (6a): Complex [{(η^6-benzene)$RuCl_2$}$_2$] (10 mg, 20 μmol) and **4a** (2.1 equiv, 42 μmol, 7.0 mg) were used. The solution turned from red to deep brown after stirring for 2 h. The product was obtained as a pale-yellow solid (80.4%, 13.8 mg) with HPLC purity (99.3%, eluent: 60% ACN/H_2O, R_t: 1.36 min). ^{1}H NMR (400 MHz, [D_6]DMSO): δ = 3.74 (s, 3H; NMe), 5.81 (s, 6H; CH-benzene), 7.86 (d, J = 8.4 Hz, 1H; NH), 8.02 (s, 1H; CH), 10.00 (d, J = 8.8 Hz, 1H; NH), 10.20 (s, 1H; NHCO), 12.71 ppm (br, 1H; NH); IR (KBr): $\tilde{\nu}$ = 3497, 3385, 3178, 2760, 1642, 1597, 1557, 1400, 1239, 844, 758 cm^{-1}; ESI-MS (MeOH): m/z: 394.9 $[M]^+$, 358.9 $[M-HCl]^+$; HRMS (ESI): m/z calcd for $[C_{12}H_{14}N_6ORuCl-HCl]^+$: 359.0194 $[M-HCl]^+$; found: 359.0192.

[(η^6-benzene)RuCl(κ^2-4f)]·Cl (6f): Complex [{(η^6-benzene)$RuCl_2$}$_2$] (10 mg, 20 μmol) and **4f** (2.1 equiv, 42 μmol, 6.4 mg) were used. The solution turned from red to deep brown after stirring for 2 h. The product was obtained as a brown solid (82.5%, 13.6 mg) with HPLC purity (98.3%, eluent: 60% ACN/H_2O, R_t: 2.14 min). ^{1}H NMR (400 MHz, [D_6]DMSO): δ = 3.96 (s, 3H; NMe), 6.02 (s, 6H; CH-benzene), 8.04 (d, J = 8.4 Hz, 1H; NH), 8.18 (s, 1H; CH), 9.04 (s, 1H; CH), 10.23 (d, J = 8.4 Hz, 1H; NH), 11.8 ppm (s, 1H; NH); IR (KBr): $\tilde{\nu}$ = 3659, 3303, 2987, 1705, 1617, 1555, 1473, 1194, 807, 759 cm^{-1}; ESI-MS (MeOH): m/z: 379.0 $[M]^+$, 342.8 $[M-HCl]^+$; HRMS (ESI): m/z calcd for $[C_{12}H_{14}N_6RuCl-HCl]^+$: 343.0245 $[M-HCl]^+$; found: 343.0232.

[(η^6-triisopropylbenzene)RuCl(κ^2-4a)]·Cl (7a): Complex [{(η^6-triisopropylbenzene)$RuCl_2$}$_2$] (10 mg, 13 μmol) and **4a** (2.1 equiv, 27 μmol, 4.9 mg) were used. The solution turned from red to deep orange after stirring for 2 h. The product was obtained as an orange solid (89.2%, 13.2 mg) with HPLC purity (99.3%, eluent: 80% ACN/H_2O, R_t: 1.75 min). ^{1}H NMR (400 MHz, [D_6]DMSO): δ = 1.21 (d, J = 6.6 Hz, 9H; Me_2CH), 1.26 (d, J = 6.6 Hz, 9H; Me_2CH), 2.90 (sep, J = 6.9 Hz, 3H; CH), 3.75 (s, 3H; NMe), 5.59 (s, 3H; CH-isopropyl benzene), 7.85 (d, J = 8.0 Hz, 1H; NH), 8.09 (s, 1H; CH), 9.64 (d, J = 8.4 Hz, 1H; NH), 10.0 (s, 1H; NHCO), 12.77 ppm (br, 1H; NH); IR (KBr): $\tilde{\nu}$ = 3529, 3258, 2872, 1726, 1655, 1588, 1421, 1246, 881, 786 cm^{-1}; ESI-MS (MeOH): m/z: 521.0 $[M]^+$, 484.7 $[M-HCl]^+$; HRMS (ESI): m/z calcd for $[C_{21}H_{32}N_6ORuCl-HCl]^+$: 485.1602 $[M-HCl]^+$; found: 485.1611.

[(η^6-triisopropylbenzene)RuCl(κ^2-4b)]·Cl (7b): Complex [{(η^6-triisopropylbenzene)$RuCl_2$}$_2$] (10 mg, 13 μmol) and **4b** (2.1 equiv, 27 μmol, 7.3 mg) were used. The solution turned from red to deep orange after stirring of 2 h. The product was obtained as a pale-yellow solid (86.4%, 14.8 mg) with HPLC purity (98.3%, eluent: 80% ACN/H_2O, R_t: 2.14 min). ^{1}H NMR (400 MHz, CD_3OD): δ = 1.20 (d, J = 6.4 Hz, 9H; Me_2CH), 1.25 (d, J = 7.2 Hz, 9H; Me_2CH), 2.89 (m, 3H; CH), 3.00 (t, J = 7.2 Hz, 2H; CH_2), 4.22 (br, 2H; CH_2), 5.57 (s, 3H; CH-isopropyl benzene), 7.05 (s, 1H; NH), 7.13–7.22 (m, 5H; Ph), 7.26 (s, 1H; NH), 7.28 (s, 1H; CH), 7.91 (s, 1H; NHCO), 9.51 ppm (d, J = 8.8 Hz, 1H; NH); IR (KBr): $\tilde{\nu}$ = 3526, 3359, 2928, 1712, 1656, 1524, 1462, 1185, 857, 787 cm^{-1}; ESI-MS (MeOH): m/z: 611.1 $[M]^+$, 574.9 $[M-HCl]^+$; HRMS (ESI): m/z calcd for $[C_{28}H_{38}N_6ORuCl-HCl]^+$: 575.2072 $[M-HCl]^+$; found: 575.2077.

[(η^6-triisopropylbenzene)RuCl(κ^2-4f)]·Cl (7f): Complex [{(η^6-triisopropylbenzene)$RuCl_2$}$_2$] (10 mg, 13 μmol) and **4f** (2.1 equiv, 27 μmol, 4.5 mg) were used. The solution turned from red to deep orange after stirring of 2 h. The product was obtained as a yellow solid (82.6%, 11.9 mg) with HPLC purity (99.8%, eluent: 80% ACN/H_2O, R_t: 2.02 min). ^{1}H NMR (400 MHz, [D_6]DMSO): δ = 1.21 (d, J = 6.8 Hz, 9H; Me_2CH), 1.27 (d, J = 6.8 Hz, 9H; Me_2CH), 2.92 (sep, J = 6.4 Hz, 3H; CH), 4.04 (s, 3H; NMe), 5.61 (s, 1H; CH-triisopropyl benzene), 7.98 (s, 1H; CH), 8.52 (s, 1H; CH), 8.76 (d, J = 8.0 Hz, 1H; NH), 9.93 (s, 1H; NH), 10.81 ppm (d, J = 8.0 Hz, 1H; NH); IR (KBr): $\tilde{\nu}$ = 3514, 3250, 2964, 1663, 1587, 1425, 1246,

894, 788 cm^{-1}; ESI-MS (MeOH): *m/z*: 505.0 $[M]^+$, 469.0 $[M-HCl]^+$; HRMS (ESI): *m/z* calcd for $[C_{21}H_{32}N_6RuCl-HCl]^+$: 469.1653 $[M-HCl]^+$; found: 469.1633; single crystals suitable for X-ray diffraction studies were obtained by vapor diffusion of diethyl ether into a saturated solution of the compound in MeOH.

[(η^6-cymene)Ru(PTA)(κ^2-4a)]·2Cl (P5a): A solution of **5a** (10 mg, 20 μmol) and PTA (1.1 equiv, 22 μmol, 3.6 mg) in MeOH turned from orange to green after stirring for 2 h. A green precipitate was obtained upon addition of diethyl ether and collected by filtration (83.2%, 11 mg) with HPLC purity (99.5%, eluent: 80% ACN/H_2O, R_t: 1.63 min). ^{1}H NMR (300 MHz, [D_6]DMSO): δ = 1.16 (d, J = 6.9 Hz, 3H; Me_2CH), 1.20 (d, J = 6.6 Hz, 3H; Me_2CH), 2.19 (s, 3H; Me), 2.73–2.80 (m, 1H; CH), 3.71 (s, 3H; NMe), 4.07 (d, J_{gem} = 13.5 Hz, 3H; CH_2), 4.30 (d, J_{gem} = 13.5 Hz, 3H; CH_2), 4.43 (s, 6H; CH_2), 5.71 (d, J = 5.7 Hz, 1H; CH-*p* cymene), 6.11 (d, J = 6.3 Hz, 1H; CH-*p* cymene), 6.21 (d, J = 6.3 Hz, 1H; CH-*p* cymene), 6.37 (br, 1H; CH-*p* cymene), 8.28 (s, 1H; CH), 9.17 (s, 1H; NHCO), 9.81 ppm (s, 1H; NH); ^{31}P{^{1}H} NMR (400Mz, [D_6]DMSO): δ = −34.5 ppm; IR (KBr): $\tilde{\nu}$ = 3477, 3261, 3149, 2970, 1659, 1537, 1420, 1284, 1151, 897, 774 cm^{-1}; ESI-MS (MeOH): *m/z*: 286.3 $[M]^{2+}$, 414.8 $[M-H-PTA]^+$; HRMS (ESI): *m/z* calcd for $[C_{22}H_{34}N_9OPRu-H-PTA]^+$: 415.0820 $[M-H-PTA]^+$; found: 415.0831.

[(η^6-cymene)Ru(PTA)(κ^2-4f)]·2Cl (P5f): A solution of **5f** (10 mg, 20 μmol) and PTA (1.1 equiv, 22 μmol, 3.6 mg) in MeOH turned from orange to green after stirring for 2 h. A green precipitate was obtained upon addition of diethyl ether and collected by filtration (86.4%, 11.5 mg) with HPLC purity (88.3%, eluent: 80% ACN/H_2O, R_t: 2.08 min). ^{1}H NMR (300 MHz, [D_6]DMSO): δ = 1.18 (d, J = 6.0 Hz, 3H; Me_2CH), 1.22 (d, J = 6.6 Hz, 3H; Me_2CH), 2.20 (s, 3H; Me), 2.78–2.84 (m, 1H; CH), 4.06 (s, 3H; NMe), 4.34–4.45 (m, 12H; CH_2), 5.80 (br, 1H; CH-*p* cymene), 6.20 (br, 1H; CH-*p* cymene), 6.42 (br, 2H; CH-*p* cymene), 8.17 (s, 1H; CH), 8.78 (s, 1H; CH), 9.56 (br, 1H; NH), 10.82 (br, 1H; NH), 11.22 ppm (br, 1H; NH); ^{31}P{^{1}H} NMR (400Mz, [D_6]DMSO): δ = −35.4 ppm; IR (KBr): $\tilde{\nu}$ = 3466, 3266, 3149, 2906, 1659, 1544, 1240, 781. cm^{-1}; ESI-MS (MeOH): *m/z*: 278.3 $[M]^{2+}$, 399.0 $[M-H-PTA]^+$; HRMS (ESI): *m/z* calcd for $[C_{22}H_{34}N_9PRu-H-PTA]^+$: 399.0871 $[M-H-PTA]^+$; found: 399.0861.

X-ray diffraction studies: X-ray data were collected with a Bruker AXS SMART APEX diffractometer using $Mo_{K\alpha}$ radiation at 223(2) K with the SMART suite of Programs.[30] Data were processed and corrected for Lorentz and polarization effects by means of SAINT software,[31] and for absorption effects using the SADABS software.[32] Structural solution and refinement were carried out by using the SHELXTL suite of programs.[33] The structure was solved by using Direct Methods. Non-hydrogen atoms were located by using difference maps and were given anisotropic displacement parameters in the final refinement. All the H atoms were put at calculated positions by means of the riding model. CCDC-900858 and CCDC-900859 contain the supplementary crystallographic data for this paper. These data can be obtained free of charge from The Cambridge Crystallographic Data Centre via www.ccdc.cam.ac.uk/data_request/cif.

Binding studies: Radioligand-binding experiments with tritiated radioligands were carried out at room temperature as described previously.[34] Competition-binding studies were carried out at a concentration of 1 nM, in saturation experiments a radioligand concentration of 0.2–10 nM was used. Nonspecific binding was determined in the presence of 1 mM theophylline for A_1AR and 100 μM (*R*)-N6-phenylisopropyladenosine (R-PIA) for A_{2A}AR and A_3AR. For the incubation and separation of bound from free ligand, a 96-well microplate filtration system (Millipore Multiscreen MAFC) was used. The K_i values were calculated from competition curves by nonlinear curve fitting with the program SCTFIT.[35] In the case of hA_{2B}AR, adenylyl cyclase experiments were carried out as described previously with minor modifications.[34,36] Membranes transfected with hA_{2B} receptor were incubated with 100 nM NECA and 150000 cpm of [α-^{32}P]ATP and tested compounds in different concentrations for 20 min in the incubation mixture without ethylene glycol tetraacetic acid (EGTA) and NaCl. The K_i values for the concentration-dependent inhibition of NECA-mediated adenylyl cyclase activity caused by tested antagonists were calculated accordingly.

Acknowledgements

This work was supported by the National University of Singapore and Singapore Ministry of Education (MOE2009-T2–2–011 and R-398–000–068–112 to G.P. and R-143–000–411–133 and R-143–000–512–112 to W.H.A.). The authors acknowledge support by A*STAR-SERC TSRP-iNPB 102 152 0016. The authors thank Sonja Kachler for her assistance and expertise in the pharmacological evaluation of the compounds.

[1] a) K. A. Jacobson, P. J. van Galen, M. Williams, *J. Med. Chem.* **1992**, *35*, 407–422; b) C. E. Müller, T. Scior, *Pharm. Acta Helv.* **1993**, *68*, 77–111; c) Q. Y. Zhou, C. Li, M. E. Olah, R. A. Johnson, G. L. Stiles, O. Civelli, *Proc. Natl. Acad. Sci. USA* **1992**, *89*, 7432–7436.

[2] a) S. A. Poulsen, R. J. Quinn, *Bioorg. Med. Chem.* **1998**, *6*, 619–641; b) K. A. Jacobson, Z. G. Gao, *Nat. Rev. Drug Discovery* **2006**, *5*, 247–264.

[3] S. Moro, Z. G. Gao, K. A. Jacobson, G. Spalluto, *Med. Res. Rev.* **2006**, *26*, 131–159.

[4] S. Gessi, K. Varani, S. Merighi, E. Cattabriga, V. Iannotta, E. Leung, P. G. Baraldi, P. A. Borea, *Mol. Pharmacol.* **2002**, *61*, 415–424.

[5] a) S. Gessi, E. Cattabriga, A. Avitabile, R. Gafa, G. Lanza, L. Cavazzini, N. Bianchi, R. Gambari, C. Feo, A. Liboni, S. Gullini, E. Leung, S. Mac-Lennan, P. A. Borea, *Clin. Cancer Res.* **2004**, *10*, 5895–5901; b) L. Madi, A. Ochaion, L. Rath-Wolfson, S. Bar-Yehuda, A. Erlanger, G. Ohana, A. Harish, O. Merimski, F. Barer, P. Fishman, *Clin. Cancer Res.* **2004**, *10*, 4472–4479.

[6] S. L. Cheong, S. Federico, G. Venkatesan, A. L. Mandel, Y. M. Shao, S. Moro, G. Spalluto, G. Pastorin, *Med. Res. Rev.* **2013**, *33*, 235–335.

[7] a) J. Jiang, A. M. van Rhee, L. Chang, A. Patchornik, X. D. Ji, P. Evans, N. Melman, K. A. Jacobson, *J. Med. Chem.* **1997**, *40*, 2596–2608; b) J. L. Jiang, A. M. van Rhee, N. Melman, X. D. Ji, K. A. Jacobson, *J. Med. Chem.* **1996**, *39*, 4667–4675; c) A. H. Li, S. Moro, N. Forsyth, N. Melman, X. D. Ji, K. A. Jacobson, *J. Med. Chem.* **1999**, *42*, 706–721; d) A. H. Li, S. Moro, N. Melman, X. D. Ji, K. A. Jacobson, *J. Med. Chem.* **1998**, *41*, 3186–3201; e) A. M. van Rhee, J. L. Jiang, N. Melman, M. E. Olah, G. L. Stiles, K. A. Jacobson, *J. Med. Chem.* **1996**, *39*, 2980–2989.

[8] a) X. D. Ji, N. Melman, K. A. Jacobson, *J. Med. Chem.* **1996**, *39*, 781–788; b) Y. Karton, J. L. Jiang, X. D. Ji, N. Melman, M. E. Olah, G. L. Stiles, K. A. Jacobson, *J. Med. Chem.* **1996**, *39*, 2293–2301; c) S. Moro, A. M. van Rhee, L. H. Sanders, K. A. Jacobson, *J. Med. Chem.* **1998**, *41*, 46–52.

[9] a) J. E. van Muijlwijk-Koezen, H. Timmerman, R. Link, H. van der Goot, I. J. AP, *J. Med. Chem.* **1998**, *41*, 3987–3993; b) J. E. van Muijlwijk-Koezen, H. Timmerman, R. Link, H. van der Goot, A. P. Ijzerman, *J. Med. Chem.* **1998**, *41*, 3994–4000; c) J. E. van Muijlwijk-Koezen, H. Timmerman, H. van der Goot, W. M. Menge, J. Frijtag Von Drabbe Kunzel, M. de Groote, I. J. AP, *J. Med. Chem.* **2000**, *43*, 2227–2238.

[10] a) Y. C. Kim, M. de Zwart, L. Chang, S. Moro, J. K. von Frijtag Drabbe Kunzel, N. Melman, I. J. AP, K. A. Jacobson, *J. Med. Chem.* **1998**, *41*, 2835–2845; b) Y. C. Kim, X. D. Ji, K. A. Jacobson, *J. Med. Chem.* **1996**, *39*, 4142–4148.

[11] P. G. Baraldi, M. A. Tabrizi, D. Preti, A. Bovero, F. Fruttarolo, R. Romagnoli, N. A. Zaid, A. R. Moorman, K. Varani, P. A. Borea, *J. Med. Chem.* **2005**, *48*, 5001–5008.

[12] P. G. Baraldi, B. Cacciari, R. Romagnoli, G. Spalluto, S. Moro, K. N. Klotz, E. Leung, K. Varani, S. Gessi, S. Merighi, P. A. Borea, *J. Med. Chem.* **2000**, *43*, 4768–4780.

[13] S. L. Cheong, A. Dolzhenko, S. Kachler, S. Paoletta, S. Federico, B. Cacciari, K. N. Klotz, S. Moro, G. Spalluto, G. Pastorin, *J. Med. Chem.* **2010**, *53*, 3361–3375.

[14] a) E. Meggers, *Chem. Commun.* **2009**, 1001–1010; b) S. P. Mulcahy, E. Meggers, *Top. Organomet. Chem.* **2010**, *32*, 141–153.

[15] a) G. E. Atilla-Gokcumen, N. Pagano, C. Streu, J. Maksimoska, P. Filippakopoulos, S. Knapp, E. Meggers, *ChemBioChem* **2008**, *9*, 2933–2936; b) J. Maksimoska, L. Feng, K. Harms, C. Yi, J. Kissil, R. Marmorstein, E. Meggers, *J. Am. Chem. Soc.* **2008**, *130*, 15764–

15765; c) N. Pagano, J. Maksimoska, H. Bregman, D. S. Williams, R. D. Webster, F. Xue, E. Meggers, *Org. Biomol. Chem.* **2007**, *5*, 1218–1227.
[16] a) H. Bregman, P. J. Carroll, E. Meggers, *J. Am. Chem. Soc.* **2006**, *128*, 877–884; b) E. Meggers, G. E. Atilla-Gokcumen, H. Bregman, J. Maksimoska, S. P. Mulcahy, N. Pagano, D. S. Williams, *Synlett* **2007**, *8*, 1177–1189.
[17] a) M. Patra, G. Gasser, M. Wenzel, K. Merz, J. E. Bandow, N. Metzler-Nolte, *Organometallics* **2012**, *31*, 5760–5771; b) M. Patra, G. Gasser, M. Wenzel, K. Merz, J. E. Bandow, N. Metzler-Nolte, *Organometallics* **2010**, *29*, 4312–4319; c) M. Patra, G. Gasser, A. Pinto, K. Merz, I. Ott, J. E. Bandow, N. Metzler-Nolte, *ChemMedChem* **2009**, *4*, 1930–1938.
[18] W. H. Ang, L. J. Parker, A. De Luca, L. Juillerat-Jeanneret, C. J. Morton, M. Lo Bello, M. W. Parker, P. J. Dyson, *Angew. Chem.* **2009**, *121*, 3912–3915; *Angew. Chem. Int. Ed.* **2009**, *48*, 3854–3857.
[19] J. X. Ong, C. W. Yap, W. H. Ang, *Inorg. Chem.* **2012**, *51*, 12483–12492.
[20] a) G. Gasser, N. Metzler-Nolte, *Curr. Opin. Chem. Biol.* **2012**, *16*, 84–91; b) M. Patra, G. Gasser, N. Metzler-Nolte, *Dalton Trans.* **2012**, *41*, 6350–6358.
[21] a) C. G. Hartinger, N. Metzler-Nolte, P. J. Dyson, *Organometallics* **2012**, *31*, 5677–5685; b) C. G. Hartinger, P. J. Dyson, *Chem. Soc. Rev.* **2009**, *38*, 391–401; c) P. C. Bruijnincx, P. J. Sadler, *Adv. Inorg. Chem.* **2009**, *61*, 1–62.
[22] a) C. Scolaro, A. Bergamo, L. Brescacin, R. Delfino, M. Cocchietto, G. Laurenczy, T. J. Geldbach, G. Sava, P. J. Dyson, *J. Med. Chem.* **2005**, *48*, 4161–4171; b) A. Bergamo, A. Masi, P. J. Dyson, G. Sava, *Int. J. Oncol.* **2008**, *33*, 1281–1289; c) A. Bergamo, B. Gava, E. Alessio, G. Mestroni, B. Serli, M. Cocchietto, S. Zorzet, G. Sava, *Int. J. Oncol.* **2002**, *21*, 1331–1338; d) G. Sava, R. Gagliardi, A. Bergamo, E. Alessio, G. Mestroni, *Anticancer Res.* **1999**, *19*, 969–972.
[23] a) C. G. Hartinger, S. Zorbas-Seifried, M. A. Jakupec, B. Kynast, H. Zorbas, B. K. Keppler, *J. Inorg. Biochem.* **2006**, *100*, 891–904; b) R. E. Morris, R. E. Aird, P. D. Murdoch, H. M. Chen, J. Cummings, N. D. Hughes, S. Parsons, A. Parkin, G. Boyd, D. I. Jodrell, P. J. Sadler, *J. Med. Chem.* **2001**, *44*, 3616–3621; c) A. Habtemariam, M. Melchart, R. Fernandez, S. Parsons, I. D. H. Oswald, A. Parkin, F. P. A. Fabbiani, J. E. Davidson, A. Dawson, R. E. Aird, D. I. Jodrell, P. J. Sadler, *J. Med. Chem.* **2006**, *49*, 6858–6868.
[24] a) W. H. Ang, A. Casini, G. Sava, P. J. Dyson, *J. Organomet. Chem.* **2011**, *696*, 989–998; b) W. H. Ang, P. J. Dyson, *Eur. J. Inorg. Chem.* **2006**, 4003–4018.
[25] A. V. Dolzhenko, G. Pastorin, A. V. Dolzhenko, W. K. Chui, *Tetrahedron Lett.* **2009**, *50*, 5617–5621.
[26] C. S. Allardyce, P. J. Dyson, D. J. Ellis, S. L. Heath, *Chem. Commun.* **2001**, 1396–1397.
[27] a) A. F. A. Peacock, A. Habtemariam, S. A. Moggach, A. Prescimone, S. Parsons, P. J. Sadler, *Inorg. Chem.* **2007**, *46*, 4049–4059; b) F. Wang, H. M. Chen, S. Parsons, L. D. H. Oswald, J. E. Davidson, P. J. Sadler, *Chem. Eur. J.* **2003**, *9*, 5810–5820; c) C. Scolaro, C. G. Hartinger, C. S. Allardyce, B. K. Keppler, P. J. Dyson, *J. Inorg. Biochem.* **2008**, *102*, 1743–1748; d) Y. Q. Tan, P. J. Dyson, W. H. Ang, *Organometallics* **2011**, *30*, 5965–5971.
[28] a) H. Petzold, J. Xu, P. J. Sadler, *Angew. Chem.* **2008**, *120*, 3050–3053; *Angew. Chem. Int. Ed.* **2008**, *47*, 3008–3011; b) T. Sriskandakumar, H. Petzold, P. C. Bruijnincx, A. Habtemariam, P. J. Sadler, P. Kennepohl, *J. Am. Chem. Soc.* **2009**, *131*, 13355–13361.
[29] a) M. A. Bennett, A. K. Smith, *J. Chem. Soc. Dalton Trans.* **1974**, 233–241; b) A. Astarina, M. J. Chow, W. H. Ang, *Aust. J. Chem.* **2012**, *65*, 1271–1276.
[30] Bruker AXS Inc., SMART version 5.628, Madison, WI, **2001**.
[31] Bruker AXS Inc., SAINT+ version 6.22a, Madison, WI, **2001**.
[32] SADABS version 2.10, University of Gottingen, **2001**.
[33] Bruker AXS Inc., SHELXTL version 6.14, Madison, WI, **2000**.
[34] K. N. Klotz, J. Hessling, J. Hegler, C. Owman, B. Kull, B. B. Fredholm, M. J. Lohse, *Naunyn Schmiedebergs Arch. Pharmacol.* **1998**, *357*, 1–9.
[35] A. D. Lean, A. A. Hancock, R. J. Lefkowitz, *Mol. Pharmacol.* **1982**, *21*, 5–16.
[36] K. N. Klotz, G. Cristalli, M. Grifantini, S. Vittori, M. J. Lohse, *J. Biol. Chem.* **1985**, *260*, 14659–14664.

Received: September 14, 2012
Revised: January 15, 2013
Published online: ■■ ▮▮, 0000

Scaffold design: A novel class of ruthenium(II)–arene complexes containing chelating *N*,*N*-pyrazolo–pyrimidine ligands was rationally developed to be selective antagonists of human A_3 adenosine receptors based on the proven pyrazolo–triazolo–pyrimidine design (see figure).

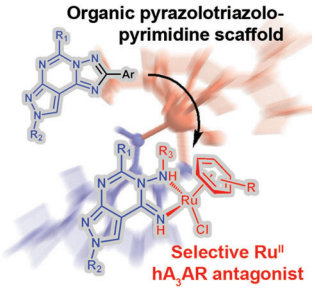

Inhibitors

P. Paira, M. J. Chow, G. Venkatesan, V. K. Kosaraju, S.-L. Cheong, K.-N. Klotz, W. H. Ang, G. Pastorin** ..... ▮▮▮▮–▮▮▮▮

Organoruthenium Antagonists of Human A_3 Adenosine Receptors